International Journal of Modern Physics A
Vol. 36, Nos. 11 & 12 (2021) 2140011 (13 pages)

DOI: 10.1142/S0217751X2140011X

Performance tests and simulations for Taiji-1 inertial sensor

Jian Min[*], Jun-Gang Lei[*,¶], Yun-Peng Li[*], Dong-Xue Xi[*], Wen-Ze Tao[*], Cun-Hui Li[*], Xiao-Qing Zhang[*], Zuo-Lei Wang[*,‖], Da Fan[†], Zi-Ren Luo[‡], Jun-Biao Wang[‡], Zhi Wang[§], Ke-Qi Qi[§]

[*]*National Key Laboratory of Science and Technology on Vacuum Technology and Physics, Lanzhou Institute of Space Technology and Physics, Lanzhou, China*

[†]*Qian Xuesen Laboratory of Space Technology, Beijing, China*

[‡]*Institute of Mechanics, Chinese Academy of Sciences, Beijing, China*

[§]*Changchun Institute of Optics, Chinese Academy of Sciences, Changchun, China*
[¶]*Lei7412@163.com*
[‖]*wzlgam2000@163.com*

[**]*On behalf of The Taiji Scientific Collaboration*

Received 15 September 2020
Revised 16 October 2020
Accepted 30 October 2020
Published 9 April 2021

Taiji-1 satellite was successfully launched on 31 August 2019, and it has been operating normally in orbit until now. A series of in-orbit experiments were carried out with the inertial sensor, which included the micro-thrust test, drag-free control test and laser interferometer test. Comprehensive performance simulations and tests of the inertial sensor were also carried out prior to the launch of Taiji-1, including the calibration and drop-tower tests. These tests were one of the preconditions for the success of these experiments. The calibration experiments were conducted in a cave-lab using the gravity-inclination method and the scale factors of the inertial sensor along Y- and Z-axis were measured. In addition, 20 drop-tower tests were carried out in the National Microgravity Laboratory of China (NMLC) drop tower and the control stability of all the axes was tested and optimized. A simulation model was used before each test, and the results showed that an accurate simulation prior to each experiment had an important role in ensuring the efficiency and accuracy of the experiment. The circuit-gain switch was realized for the first time during the drop-tower tests. The test results indicated that the microgravity level of the NMLC drop tower could reach about 13 μg_0 along the horizontal axes, offering an important reference for researchers planning to conduct microgravity experiments in the NMLC drop tower.

Keywords: Taiji-1 inertial sensor; performance; calibration experiments; simulation.

1. Introduction

Taiji-1 is the first technical verification satellite of China's Space Gravitational Wave Detection Program.[1] Its aim is to investigate the key technologies used in space gravitational wave detection,[2–5] including the high precision displacement and acceleration detection and control technology, micro-thrust technology, drag-free control and laser interferometer technology.[6–10]

[¶,‖]Corresponding authors.
[**]For more details, please refer to article 2102002 of this Special Issue.

The inertial sensor is one of the main payloads on the Taiji-1 satellite, and is mainly used for measuring the micro-displacement and acceleration of the satellite. In the drag-free experiment, the inertial sensor provides the satellite's micro-displacement as an input to the micro-thruster. Furthermore, in the laser interference test, the test mass of the inertial sensor provides a reflection mirror for the laser beams, and its control stability strongly influences the test accuracy.

The premise for the success of the Taiji-1 satellite is the stability and quality of the inertial sensor. Therefore, it is important to fully evaluate all types of performance of the inertial sensor under ground conditions as well as accurately simulate the on-orbit performance.

The gravitational acceleration of 1 g_0 (9.8 m/s^2) on earth significantly exceeds the operating range of the inertial sensor (1×10^{-3} g_0). Consequently, it is necessary to apply a high voltage of nearly 1000 V along the X-axis of the sensor head and levitate the test mass for further tests. By adjusting the tilt angle of the test platform, the test mass could be controlled in the center of the electrode house and subsequently, the scale factors, range and capture ability in the horizontal axis could be measured.

On the other hand, it is not possible to evaluate the performance of the inertial sensor along the X-axis in a normal laboratory setup due to the high-voltage suspension. To ensure the in-orbit performance, the drop tower of the National Microgravity Laboratory of China (NMLC) in Beijing[11,12] was used. This tower can provide a microgravity environment for testing and optimizing the control stability along all the axes.[13–17]

The feedback-voltage (V_f) and bias-voltage (V_p) were properly amplified to adapt to the residual acceleration on the ground, resulting in a better control capability during the tests. Furthermore, by using the simulation model prior to all the tests, the actual control process and the effect of circuit-gain switch during the drop-tower tests were simulated in advance to get more reliable results. The experimental results showed that a proper simulation had an immense reference value for the ground test and would be necessary for successful drop-tower test.

2. The Inertial Sensor

The inertial sensor consists of a sensor head and a measure-control unit (MCU), connected via coaxial cables. The vacuum structure of the sensor head was adjusted according to different requirements of ground calibration test, drop-tower test and in-orbit test, as shown in Fig. 1.

Fig. 1(a) shows the sensor head used in the ground test. It is mainly composed of a sensor core and a vacuum structure. On the other hand, a substitute inertial sensor (SIS) (Fig. 1(b)) was used in the drop-tower test to ensure the safety of the real inertial sensor (Fig. 1(c)). Both sensors had almost similar structures with only difference being the vacuum structure on the top of the sensor head. The vacuum structure was used to maintain vacuum on the ground, while it was removed in the in-orbit sensor and the vacuum in space was used. Moreover, the SIS and the inertial sensor on Taiji-1 had the

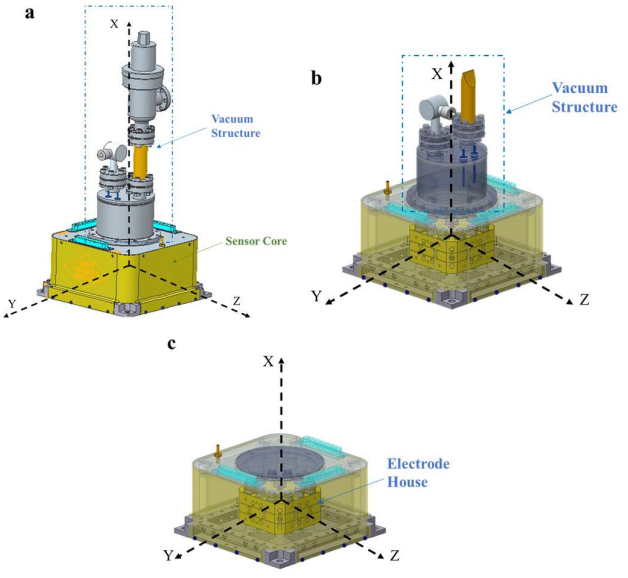

Fig. 1. (a) On-ground state. (b) Drop-tower state. (c) In-orbit state.

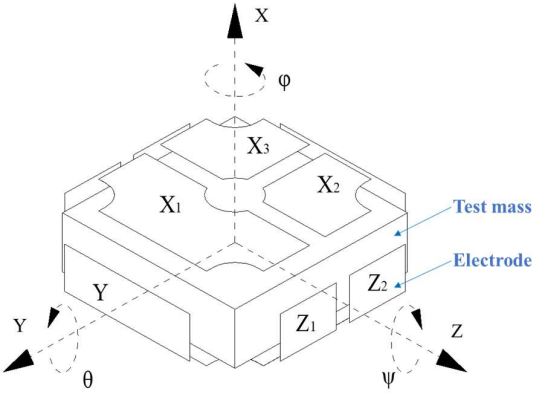

Fig. 2. Axial diagram of the electrode house.

same circuit design, and in order to adapt to the microgravity level of the drop tower, the amplifier circuit gain was adjusted. Fig. 2 shows the electrode house and the axial diagram of the sensor head. There were three, two and one electrode pairs along the *X*-, *Z*- and *Y*-axis, respectively.

A cuboid-shaped gold-plated titanium alloy was used as the test mass to gauge the acceleration of the sensor. The test mass was provided with a DC bias voltage (V_p) and a position detection AC signal (V_d) via a gold wire connected to the MCU. The electrode house surrounding the test mass was made of gold-plated microcrystalline glass for the

thermal stability and magnetic susceptibility of the sensor. With the vacuum sealing structure of the SIS, the internal vacuum of the electrode house can be maintained below 10^{-5} Pa on the ground.

The displacement signal of the test mass was obtained by measuring the capacitance difference between the test mass and electrodes. Simultaneously, a PID controller was used to ensure that the test mass was positioned at the center of the electrode house, and the acceleration of the sensor head was measured via the feedback voltages.

3. Simulation Model

During the ground test, to move the test mass to the center of the electrode house and have a stable control, it would take a lot of time to fine-tune the PID controller parameters. In addition, due to the complex equipment used in the drop-tower test, the installation process took more than half a day while the effective test time lasts only about 3.5 s. If the pre-defined control parameter values are not suitable, the test will fail, resulting in all the preparatory work being wasted. Therefore, a simulation model was used prior to each performance test for simulating the control process of the system and finding the optimal parameters. The experimental parameters were fine-tuned and modified according to the simulation results. The simulation process increased the efficiency and accuracy of the whole experiment.

The uniaxial simulation model for the drop-tower test is illustrated in Fig. 3. Different parameters used in the figure are as follows: a_{ext} and a_{mass} are the external residual acceleration and the acceleration produced by the electrostatic force, respectively, x_{mass} represents the displacement of the test mass, while U_o, U_X, U_{PID} and V_f are the output voltage of the charge amplifier, displacement voltage of the test mass, voltage provided by the PID controller and feedback voltage on the electrodes, respectively.

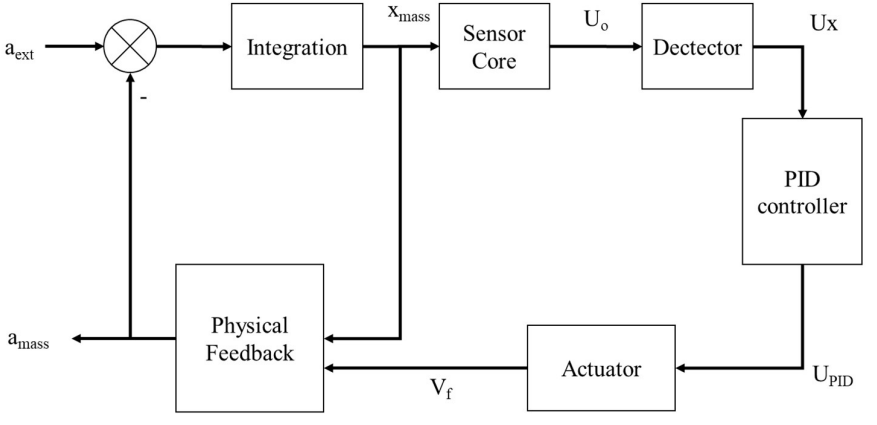

Fig. 3. Uniaxial simulation model.

In the simulation model, the noise, gain and delay in the real circuit were considered. The displacement x_{mass} was converted into the output voltage (U_o). Subsequently, U_o was further processed by the detector to obtain the specific displacement value of the test mass and output it as U_X.

The PID controller was used to provide a feedback voltage to the actuator for maintaining the test mass in the center of the electrode house. It was made up of proportional, differential and integral terms with the transfer function[18,19] given by Eq. (1) as follows:

$$G(s) = K_p + \frac{K_I}{s} + K_D s, \tag{1}$$

where K_p, K_I and K_D are the proportional, integral and differential term coefficients, respectively, and s is the Laplace operator. In the simulations, K_p, K_I and K_D should be fine-tuned so that a sufficient gain and phase margin could be obtained for a stable system.

The actuator was used to provide sufficient electrostatic force to the electrodes for maintaining the stability of the test mass. The electrostatic force used is shown in Eq. (2).[20,21]

$$F_{\text{el}} = 2\varepsilon_0 S \frac{V_p V_f (d^2 + x^2) - \left(V_f^2 + V_p^2 + V_d^2\right) \cdot dx}{(d^2 - x^2)^2}. \tag{2}$$

In the equation, S is the area of the electrode, ε_0 is the permittivity of vacuum, while V_p, V_f and V_d are the bias voltage, feedback voltage and detection voltage, respectively. The average distance between the electrode and test mass when the test mass is at the center of the electrode house is given by d, and x is the displacement of test mass relative to the center of the electrode house. It can be noted from Eq. (2) that the electrostatic force applied on the test mass can be calculated using the real-time feedback voltage (V_f) and displacement (x).

4. Performance Tests

4.1. *Calibration experiments*

The measured acceleration and feedback voltage can be expressed as follows:

$$a = c_0 + c_1 U + c_2 U^2 + \tilde{a}_{\text{RMS}}, \tag{3}$$

where a is the measured acceleration of the sensor head, c_0 is the deviation value, c_1 is the scale factor, c_2 is the quadratic coefficient, $\tilde{a}_{\text{RMS}}$ is the acceleration-noise of the inertial sensor, and U is the feedback voltage on the electrode.

As both $c_2 U^2$ and $\tilde{a}_{\text{RMS}}$ were negligible relative to $c_1 U$ in the calibration experiment, they can be ignored and Eq. (3) can be rewritten as

$$a = c_0 + c_1 U. \tag{4}$$

Suppose c_0 is 0, in this case, a simple multiplication of c_1 with U gives the measured acceleration of the sensor head. The theoretical value of the measured acceleration of the sensor head can be calculated using Eq. (5) as follows:

$$a = \frac{2\varepsilon_0 S}{md^2} V_p \frac{V_r}{k_r}, \tag{5}$$

where V_r is the output voltage of the MCU and k_r is the gain of the readout circuit. According to Eqs. (4) and (5), when U is replaced by V_r and c_0 is considered to be 0

$$c_1 = \frac{2\varepsilon_0 S}{md^2} V_p \frac{1}{k_r}. \tag{6}$$

The scale factor of the inertial sensor was calibrated using the gravity-inclination method. In this method, the test table is adjusted along one axis with a series of tile angles and the corresponding acceleration values can be detected by the inertial sensor. According to Eq. (4), a straight line can be drawn with respect to U and c_1. To ensure an accurate c_1, it is necessary to select a stable test table and a quiet environment during the calibration test, and it is also critical to simultaneously maintain a stable temperature and humidity.

A laboratory in a cave was used for the calibration test of the inertial sensor as shown in Fig. 4(a). The temperature stability in the cave was ±0.5°C/10 h, and the ground vibration was sufficiently small for the calibration test.

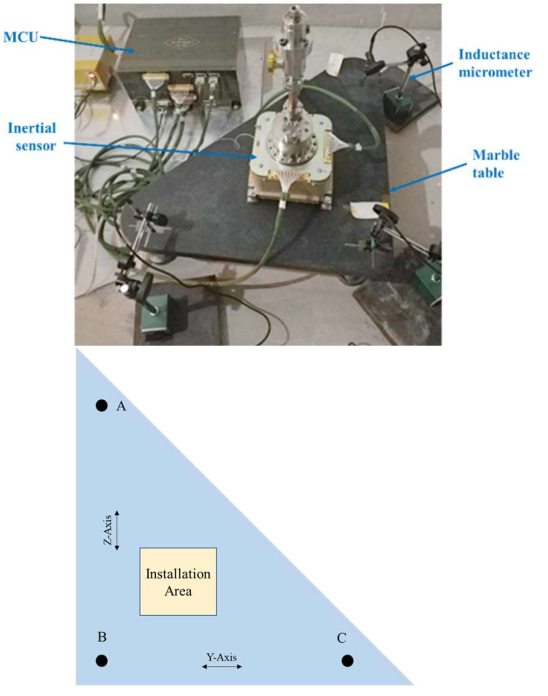

Fig. 4. (a) Calibration test in the cave laboratory. (b) Sketch of the marble-test-table.

The inertial sensor head was fixed on a marble table, and its inclination angle was adjusted through precise adjustment screws. Three inductance-micrometers, each having a resolution of 0.1 μm, were installed vertically on A, B and C, as shown in Fig. 4(b). The inclination angle of the marble-test-table can be calculated by the displacement of the inductance-micrometers and the gravity component corresponding to the inclination can be measured.

4.1.1. *Simulation results*

The control processes along the *Y*- and *Z*-axes were simulated prior to the calibration experiment and fine-tuned according to the simulation model mentioned in Sec. 3. . This ensured that the test mass could be moved to the center of the electrode house in the shortest time and remain highly stable. The initial adjustment process became easier thanks to the control parameters obtained from the simulation process. Figure 5 shows an example of the simulation results along the *Y*-axis.

As can be inferred from Fig. 5, with the control parameters obtained in the simulation process, the inertial sensor could steer the test mass to the center of the electrode house within 1 s. In addition, with an acceleration pulse of 1 mg_0 for 0.5 ms, the test mass could reach the center of the electrode house within 0.5 s. The experimental results showed that the control parameters obtained by simulations were reliable and usable in the calibration test.

4.1.2. *Calibration experiment results*

During the calibration experiment, the marble-test-table was first adjusted to a horizontal position. Subsequently, its height was adjusted by the screw along a certain axis, e.g.

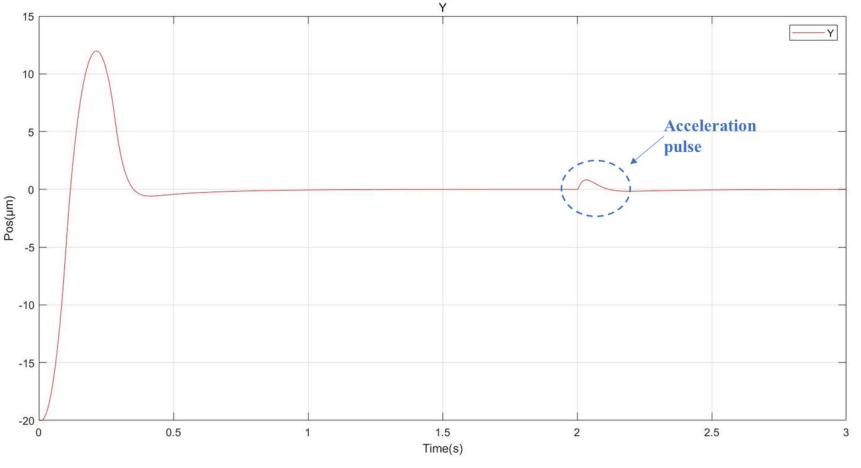

Fig. 5. Simulation curve of control process along *Y*-axis.

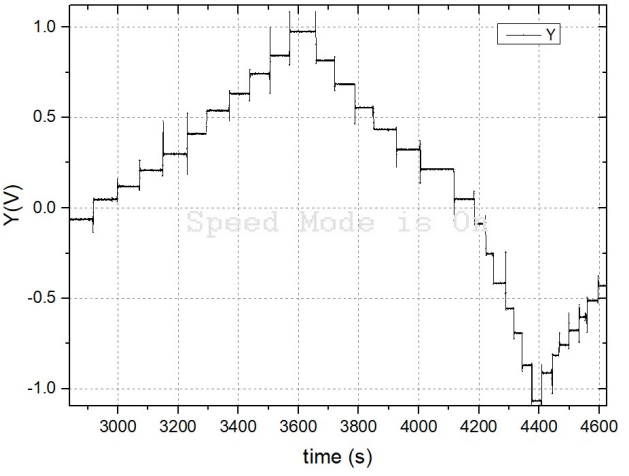

Fig. 6. Calibration curve along the *Y*-axis.

Y-axis, in a step-size of 70 μm ± 5 μm. After each adjustment, there were about 50 s for data acquisition. The acceleration value at each step was recorded at the same time. Fig. 6 shows the calibration results of the *Y*-axis. The *X*-axis and the *Y*-axis represent the calibration time and the readout voltages corresponding to the gravity component, respectively.

Based on the calibration curve shown in Fig. 6, the relationship between the gravity component and the readout voltage can be plotted. The corresponding fitting curve is shown in Fig. 7. The *X*-axis represents the readout voltages and the *Y*-axis represents the corresponding acceleration. The black square represents the actual calibration point and the red line is the least square fitting curve.

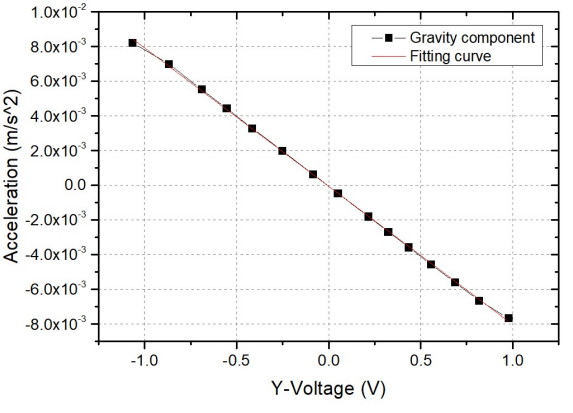

Fig. 7. Fitting curve of gravity component and readout voltage.

Table 1. Theoretical and real scale factors of *Y*- and *Z*-axes.

Axes	Gain of the read-out circuit	Theoretical scale factor ($m/s^2/V$)	Real scale factor ($m/s^2/V$)
Y	0.86	8.68×10^{-3}	7.93×10^{-3}
Z	0.87	8.95×10^{-3}	8.13×10^{-3}

The real and theoretical scale factors of *Y*- and *Z*-axes are compared in Table 1. It can be observed from the table that both scale factors are consistent with each other.

4.2. *Drop-tower experiments*

The control stability of the inertial sensor along all the axes, including the X-axis, should be evaluated before launch, to ensure the in-orbit performance. In addition, to adapt to different in-orbit microgravity levels, three control modes, namely the capture-mode, large-range mode and small-range mode should be tested. However, it was impossible to conduct such tests in a normal ground lab due to the high voltage along X-axis. The solution is to conduct systematic free-fall test.

The NMLC drop tower was used in the performance tests of the Taiji-1 inertial sensor. The tower provided a total free-fall distance and time of about 60 m and 3.5 s, respectively. Fig. 8(a) shows the placement of the SIS on the mounting plate and Fig. 8(b) illustrates the drop-tower experimental configuration. The X-axis of the SIS was parallel to the longitudinal axis of the inner capsule. In the drop-tower tests, the SIS was used to ensure safety of the real inertial sensor and the Double Capsule Mode was adopted due to its higher microgravity level of about 10^{-5} g_0.

In order to adapt to the microgravity level in the NMLC drop tower (10^{-2} mg_0), the maximum value of V_f was amplified, expanding the measurement range from ±5 μg_0 to

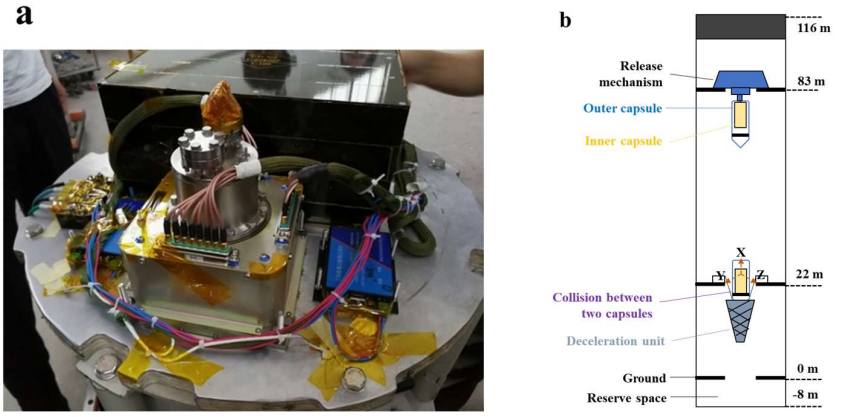

Fig. 8. (a) SIS installed on the mounting plate. (b) Sketch of the drop-tower experimental configuration.

± 0.46 mg$_0$. Three control modes were tested, namely the capture mode, large-range mode and small-range mode.

Consider the small-range mode as an example. The SIS was in the capture mode prior to the free-fall test. When the displacement voltages of all axes were within ± 0.1 V for more than 0.5 s, the mode switch took place. Consequently, V_d and V_p switched from 1 to 4 V, and from 55 to 30 V, respectively. By reducing V_p and the gain of the feedback loop, the circuit noise would be further suppressed and more accurate measurements can be achieved when the satellite's residual acceleration become smaller.

4.2.1. *Simulation results*

The preparation of one drop-tower test took about half a day. However, the test can fail if the values of the control parameters are not appropriate. To ensure the accuracy and efficiency of the test, the simulation model shown in Fig. 3 was used to simulate the stability of the control-loop and choose the best control parameters. Figure 9 shows the simulation results along *Y*-axis as an example.

According to the simulation results, the test mass was placed at the center of the electrode house in about 0.7 s after release. The mode switch occurred at 1.5 s, causing a small vibration in both displacement (blue curve labeled "Pos") and acceleration (red curve labeled "Acc") curves, as indicated by the green dotted circle in Fig. 9. The displacement curve converged to almost zero within 0.5 s after the mode switch.

All the axes simulated and optimized prior to the tests ensure that the displacement curve could converge around zero within 1 s and the displacement vibration would not be more than 1 μm after the mode switch. The experimental results demonstrated that a proper simulation before the drop test is necessary to ensure a successful test.

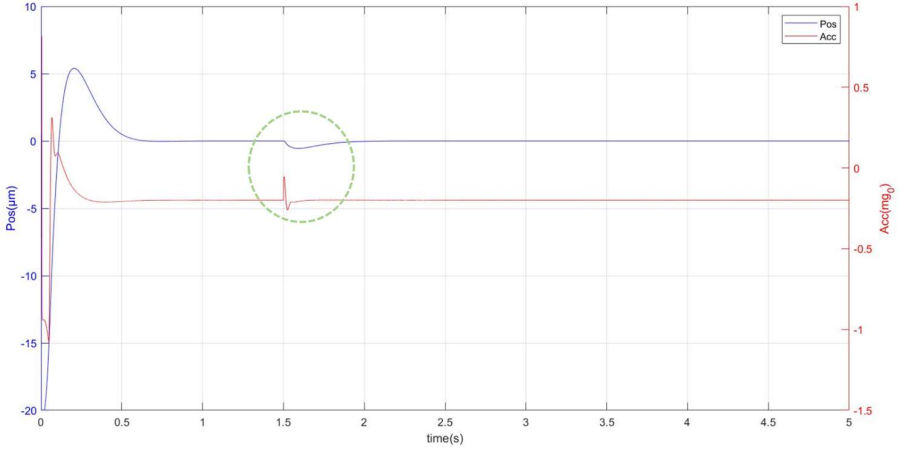

Fig. 9. Simulation results of the *Y*-axis in the small-range mode experiment.

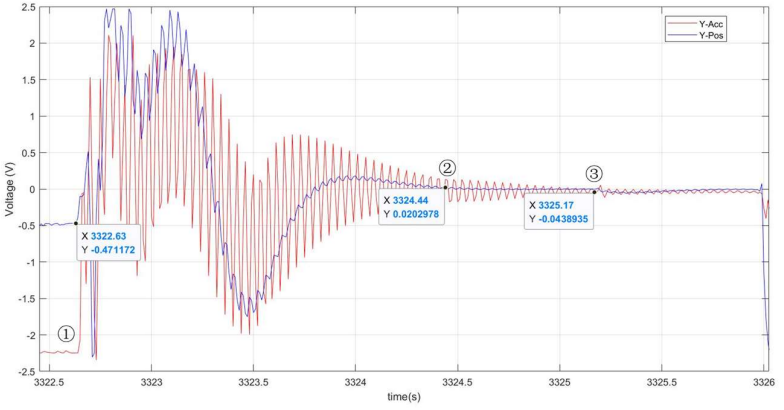

Fig. 10. Displacement and acceleration curves of the *Y*-axis.

4.2.2. *Drop-tower experiment results*

A series of drop-tower tests were conducted and a set of test methods was established, including a simulation model. The switching of different circuit gains was achieved in a drop-tower test for the first time. With the appropriate values of the control parameters, the circuit-gain switching would have a negligible effect on system stability. Fig. 10 shows the displacement and acceleration curves of the *Y*-axis during the free-fall test. The displacement and acceleration curves along *Y*-axis converged to zero from point ① to point ② in about 1.8 s. The mode switch occurred at point ③ and caused a small vibration of 0.1 V. Subsequently, the test mass was placed to the center of the electrode house in less than 1 s.

Figure 11 shows the magnified view of the *Y*-axis during the mode switch process. The green box indicates that the displacement and acceleration data along both axes remained stable before the end of the free fall.

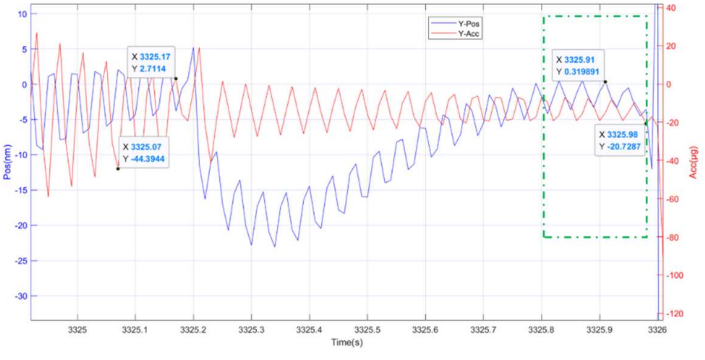

Fig. 11. Magnified view of the displacement and acceleration along the *Y*-axis in the small-range mode switch experiment.

Table 2. Displacement and acceleration data summary.

Control mode	Test item	Displacement (nm)	Acceleration (μg_0)
Capture mode	Mean value	−1	−16.4
	Maximum fluctuations	7.5	52.5
Small-range mode	Mean value	−8.1	−13.1
	Maximum fluctuations	7.7	19.5
Largest vibration during mode switch		28	61

The data within 0.1 s in both the capture mode (3325.07–3325.17s) and small-range mode (3325.55–3325.65s) shown in Fig. 11 are analyzed in Table 2. During the free-fall test, the minimum residual acceleration and the largest acceleration-vibration along the *Y*-axis were about 13 and 52.5 μg_0, respectively. At the same time, the largest displacement-vibration was only about 28 nm during the mode switch. These data indicate that once the control parameters are set correctly, the circuit-gain switch will have a negligible effect on system stability.

5. Conclusion

The performance of Taiji-1 inertial sensor was tested on the ground prior to launch. The quantitative relationship between the real acceleration of the sensor head and the readout voltage was determined based on the calibration experiments. The simulation of each axis before the calibration test could help optimize the control stability of the inertial sensor. The simulation results offered important references for obtaining the optimal controller and circuit parameters. A total of 20 free-fall tests were carried out during the drop-tower tests, and the importance of conducting simulations before the drop tests was also verified. For the first time, the switching of different circuit gains in a drop-tower test was achieved and the NMLC drop tower's residual accelerations in three dimensions were measured. The test results showed that the microgravity levels of the NMLC drop tower were about 58 and 13 μg_0 in the fall direction and along the horizontal axes, respectively.

Data Availability

The datasets generated and analyzed during the current study are available from the first author upon reasonable request.

Acknowledgment

The authors gratefully acknowledge the support by the Pre-research Project on Civil Aerospace Technologies (A0301) of CNSA. The authors declare that there are no competing interests.

References

1. W. R. Hu and Y. L. Wu, *Natl. Sci. Rev.* **4**, 685 (2017).
2. B. F. Schutz, *Class. Quantum Gravity* **13**, A219 (1996).
3. K. Danzmann *et al.*, LISA: Unveiling a hidden universe, Report No. ESA/SRE (2011), p. 3.
4. K. Danzmann *et al.*, Laser interferometer space antenna, (2017), https://arxiv.org/abs/1702.00786.
5. M. Armano *et al.*, *Phys. Rev. Lett.* **116**, 231101 (2016).
6. W. H. Ruan, Z. K. Guo, R. G. Cai and Y. Z. Zhang, Taiji program: Gravitational-wave sources (2018), https://arxiv.org/abs/1807.09495v2.
7. Z. R. Luo, Z. K. Guo, G. Jin, Y. L. Wu and W. R. Hu, *Results Phys.* **16**, 102918 (2020).
8. Z. R. Luo, H. S. Liu and G. Jin, *Opt. Laser Technol.* **105**, 146 (2018).
9. J. W. He *et al.*, *J. Propul. Technol.* **39**, 1673 (2018).
10. Y. P. Li *et al.*, *Appl. Sci.* **9**, 2087 (2019).
11. X. Q. Zhang, L. G. Yuan, W. D. Wu, L. Q. Tian and K. ZH. Yao, *Sci. China Series E-Eng. Mater. Sci.* **48**, 305 (2005).
12. T. Y. Liu, Q. P. Wu, B. Q. Sun and F. T. Han, *Sci. Rep.* **6**, 1 (2016).
13. P. Touboul and B. Foulon, *Space Forum* **4**, 145 (1998).
14. D. Bortoluzzi, B. Foulon, C. Garcı'a Marirrodriga and D. Lamarre, *Adv. Space Res.* **45**, 1358 (2010).
15. H. Selig, H. Dittus and C. Lämmerzahl, *Microgravity Sci. Technol.* **22**, 539 (2010).
16. F. Liorzou, D. Boulanger, M. Rodrigues, P. Touboul and H. Selig, *Adv. Space Res.* **54**, 1119 (2014).
17. B. Christophe *et al.*, Status of development of the future accelerometers for next generation gravity missions, *Int. Symp. Advancing Geodesy in a Changing World* (2018), pp. 85–89.
18. X. R. Mei, *Principles of Automatic Control* (Science Press, Beijing, 2005).
19. K. H. Ang, G. Chong and Y. Li, *IEEE Trans. Control Syst. Technol.* **13**, 559 (2005).
20. D. T. Xue, *J. Astronaut.* **32**, 8 (2011).
21. D. T. Xue, *Chin. J. Space Sci.* **29**, 102 (2009).